Mineralogical Magazine (2023), **87**, 433–442
doi:10.1180/mgm.2023.10

CAMBRIDGE UNIVERSITY PRESS

Article

Botuobinskite and mirnyite, two new minerals of the crichtonite group included in Cr-pyrope xenocrysts from the Internatsionalnaya kimberlite

Dmitriy I. Rezvukhin[1]*, Sergey V. Rashchenko[1,2], Igor S. Sharygin[1,3], Vladimir G. Malkovets[1,4], Taisia A. Alifirova[5], Leonid. A. Pautov[6,7], Elena N. Nigmatulina[1] and Yurii V. Seryotkin[1,2]

[1]Sobolev Institute of Geology and Mineralogy, Siberian Branch of the Russian Academy of Sciences, 3 Koptyuga Avenue, Novosibirsk 630090, Russia; [2]Novosibirsk State University, 1 Pirogova Street, Novosibirsk 630090, Russia; [3]Institute of the Earth's Crust, Siberian Branch of the Russian Academy of Sciences, 128 Lermontova Street, Irkutsk 664033, Russia; [4]ALROSA (Public Joint-Stock Company), 5 Lenina Street, Mirny 678170, Russia; [5]Department of Lithospheric Research, University of Vienna, Josef-Holaubek-Platz 2/UZA2, Vienna 1090, Austria; [6]Fersman Mineralogical Museum of the Russian Academy of Sciences, 18-2 Leninskiy Avenue, 119071 Moscow, Russia; and [7]Institute of Mineralogy, South Urals Research Center of Mineralogy and Geoecology, Uralian Branch of the Russian Academy of Sciences, Miass 456317, Russia

Abstract

Two new mineral species of the crichtonite group: botuobinskite, ideally $SrFe^{2+}(Ti_{12}^{4+}Cr_6^{3+})Mg_2[O_{36}(OH)_2]$ and mirnyite, ideally $SrZr(Ti_{12}^{4+}Cr_6^{3+})Mg_2O_{38}$, occur as inclusions in mantle-derived Cr-pyrope xenocrysts from the Internatsionalnaya kimberlite pipe, Mirny field, Siberian craton. Botuobinskite forms needle- and blade-like acicular crystals up to 1 mm in length and up to 30 μm in diameter, a large platy inclusion (700 × 700 × 80 μm) and roughly isometric grains (up to 80 μm). Mirnyite occurs as needle-and blade-like elongated inclusions (up to 1 mm). Both minerals are jet-black, opaque and exhibit a metallic lustre. In plane-polarised reflected light, botuobinskite and mirnyite are greyish-white with a weak brownish tint. Between crossed polars, the new species show distinct anisotropy in shades of bluish grey to greenish-brown. Neither bireflectance nor pleochroism is observed. Calculated densities for botuobinskite and mirnyite are 4.3582(5) and 4.3867(3) gm/cm^3, respectively. The crystal structures of botuobinskite and mirnyite have been refined ($R = 0.0316$ and 0.0285, respectively) from single crystal X-ray diffraction data. The minerals are trigonal, crystallise in the space group $R\bar{3}$ (No. 148) and are isostructural with other members of the crichtonite group. The unit cell parameters are $a =$ 10.3644(8) Å, $c = 20.6588(11)$ Å and $V = 1921.9(2)$ Å^3 for botuobinskite and $a = 10.3734(8)$ Å, $c = 20.6910$ (12) Å and $V = 1928.2(2)$ Å^3 for mirnyite, with $Z = 3$ for both. The Raman spectra of the minerals show strong peaks at 133, 313 and 711 cm^{-1}. Infrared spectroscopy data for botuobinskite indicates H–O stretching of the hydroxyl groups. Botuobinskite and mirnyite have been approved by the IMA–CNMNC under the numbers 2018-143a and 2018-144a, respectively. Botuobinskite and mirnyite are named after the Botuobinskaya exploration expedition and Mirny town, respectively. The minerals may be considered as crystal-chemical analogues of other crichtonite-group species occurring in the lithospheric mantle (i.e. loveringite, lindsleyite and mathiasite). Both species commonly occur in intimate association with Cr-pyrope as well as other peridotitic minerals and exert an important control on the partitioning of incompatible elements during mantle metasomatism.

Keywords: botuobinskite, mirnyite, new mineral, crichtonite group, inclusion, pyrope, kimberlite, Internatsionalnaya pipe, Siberian craton

(Received 2 August 2022; accepted 20 January 2023; Accepted Manuscript published online: 10 February 2023; Associate Editor: Irina O Galuskina)

Introduction

The crichtonite group includes a series of complex Fe–Ti-rich oxides (also V-rich paseroite; Mills *et al.*, 2012) with the general crystal-chemical formula $^{XII}A^{VI}B^{VI}C_{18}^{IV}T_2\Phi_{38}$, where major cations are: ^{XII}A = K, Ba, Sr, Ca, Na, La, Ce and Pb; ^{VI}B = Mn, Y, U, Fe, Zr and Sc; $^{VI}C_{18}$ = Ti, Fe, Cr, V, Nb, Mn and Al; $^{IV}T_2$ = Fe, Mg, Zn and Mn; and Φ = O, OH and F (superscript Roman numerals indicate coordination numbers; e.g. Orlandi *et al.*, 1997).

Over the last few years, we have been comprehensively investigating a suite of Cr-rich pyrope xenocrysts picked up from the heavy-mineral concentrates of the highly diamondiferous middle Palaeozoic Internatsionalnaya kimberlite pipe, Mirny field, Siberian craton. A remarkable feature of these pyrope samples is the occurrence of abundant Ti-rich oxide mineral inclusions, such as Cr- and Cr–Nb-rutile, Mg-rich ilmenite and complex chromium titanates of the crichtonite group (Malkovets *et al.*, 2016; Rezvukhin *et al.*, 2016a, 2016b, 2018). The latter are of particular interest due to their capability to incorporate a wide array of trace elements that are incompatible in common mantle minerals (e.g. silicates). The first occurrence of titanate

*Author for correspondence: Dmitriy I. Rezvukhin, Email: m.rezvukhin@igm.nsc.ru, m.rezvukhin@gmail.com

Cite this article: Rezvukhin D.I., Rashchenko S.V., Sharygin I.S., Malkovets V.G., Alifirova T.A., Pautov L.A., Nigmatulina E.N. and Seryotkin Y.V. (2023) Botuobinskite and mirnyite, two new minerals of the crichtonite group included in Cr-pyrope xenocrysts from the Internatsionalnaya kimberlite. *Mineralogical Magazine* **87**, 433–442. https://doi.org/10.1180/mgm.2023.10

inclusions compositionally similar to crichtonite-group minerals in Internatsionalnaya pyropes was documented as early as 1996 (Varlamov *et al.*, 1996). Further mineralogical examination of titanate minerals encapsulated in the pyrope xenocrysts from our collection has proved the affinity of these complex oxides to the crichtonite group (Rezvukhin *et al.*, 2018). The crichtonite-group minerals studied are chromium-enriched Zr–Al-bearing phases dominated by Ca, Sr and in a few cases Ba in the *A* site, showing compositional similarities to other crichtonite-group species that occur in the lithospheric mantle (i.e. loveringite, lindsleyite and mathiasite). However, specific details of their crystal-chemistry promoted more detailed research. In particular, Rezvukhin *et al.* (2018) suggested the Sr-specific crichtonite-group minerals could represent new members of the crichtonite group, based on their unique combination of dominant cations.

Note that prior to 1997 only *A*-site cation occupancy was considered when discriminating among species of the crichtonite series (according to the formula $AM_{21}O_{38}$; e.g. Grey *et al.*, 1976). As the compositional data for the crichtonite family expanded, the necessity for changes in the outdated nomenclature became clear. In the modern nomenclature (introduced by Orlandi *et al.*, 1997), the occupancies of four different structural sites are employed for mineral identification (the *M3*, *M4* and *M5* sites are still grouped together under the common '*C* site' because of their similarity). This approach resulted in an increase in the number of approved crichtonite-group members and allowed a greater flexibility in the identification of minerals, which may occur in a variety of paragenetic settings (magmatic, metasomatic, metamorphic and hydrothermal) and thus show an extremely diverse range of compositions with only Fe and Ti always being present.

In accordance with the updated crichtonite-group systematics, here we introduce two new Sr-characteristic mineral species of the crichtonite group: botuobinskite and mirnyite. These minerals are fairly similar in appearance, composition and physical properties; they differ, however, in the occupancy of the *B* site. Both new species and their names (symbols Btb and Mny) have been approved by the Commission on New Minerals, Nomenclature and Classification (CNMNC) of the International Mineralogical Association (IMA), under the numbers 2018-143a (Rezvukhin *et al.*, 2020a) and 2018-144a (Rezvukhin *et al.*, 2020b), respectively. The holotype specimens of botuobinskite and mirnyite are stored at the Central Siberian Geological Museum, Sobolev Institute of Geology and Mineralogy, Siberian Branch of the Russian Academy of Sciences, Novosibirsk, Russia, under the catalogue numbers VII-99/1 and VII-100/1, respectively. Botuobinskite is named in honour of members of the Botuobinskaya exploration expedition (founded in 1959), who discovered several prominent kimberlite diamond deposits in Yakutia, Russia, including the Internatsionalnaya kimberlite pipe in 1969. Mirnyite is named after Mirny town (the 'diamond capital' of Yakutia, the administrative centre of Mirninsky District), which is located close to the Internatsionalnaya kimberlite pipe, and also after the namesake Mirny kimberlite field.

Sample location and general description

The Mirny kimberlite field comprises seven diamondiferous kimberlite pipes (Internatsionalnaya, Mir, Sputnik, Amakinskaya, 23rd Party Congress, Dachnaya and Taezhnaya), emplaced in the middle Palaeozoic at ~360 Ma (Sobolev *et al.*, 1997; Kiselev *et al.*, 2014; Malkovets *et al.*, 2016; Skuzovatov *et al.*, 2016; Agashev *et al.*, 2018). This area represents a stable ancient craton core featuring a thick diamondiferous keel (Griffin *et al.*, 1999a). The two mantle-derived Cr-pyrope xenocrysts hosting inclusions of the new minerals (INT-15 and INT-66; Fig. 1) are a subset of a large collection of pyrope grains (>200) with mineral inclusions picked from the heavy-mineral concentrate of the Internatsionalnaya kimberlite. The Cr-pyrope grains examined are of lherzolitic paragenesis and show concave-upwards (normal) chondrite-normalised REE patterns (Rezvukhin *et al.*, 2018). These samples are considered as common lherzolitic garnets; they exhibit no particular features apart from hosting the inclusions of the new minerals.

Botuobinskite forms needle- and blade-like acicular inclusions up to 1 mm in length and up to 30 μm in diameter, a large platy inclusion (700 × 700 × 80 μm) and roughly isometric grains (up to 80 μm). Mirnyite occurs as needle-and blade-like elongated crystals (up to 1 mm) similar to those of botuobinskite (Fig. 1). Within the host pyrope xenocryst, mirnyite is associated with a picroilmenite inclusion, whereas botuobinskite is a single mineral in pyrope INT-15. Within the pyrope population from

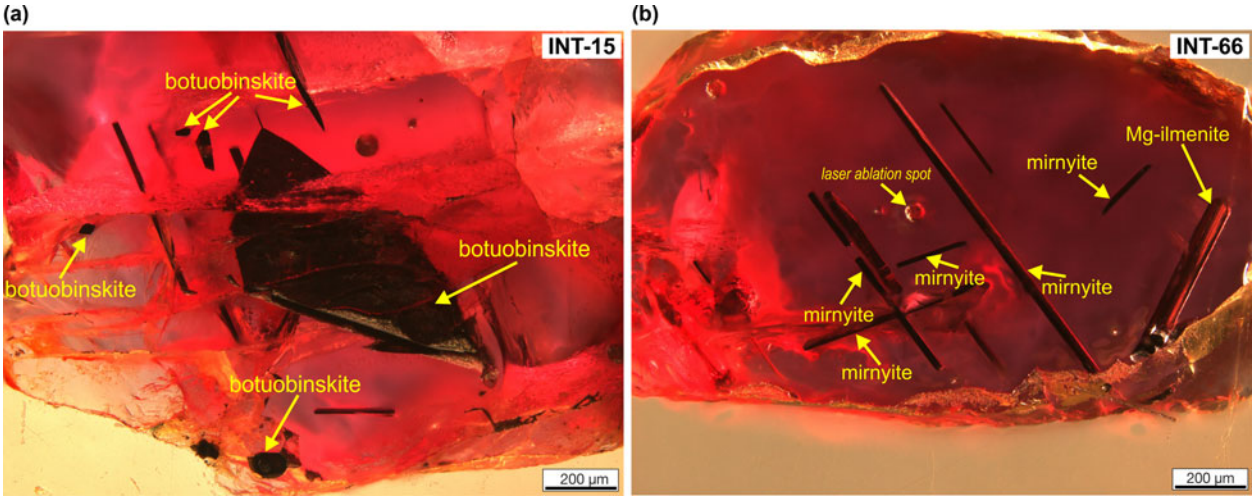

Fig. 1. Inclusions of botuobinskite (a) and mirnyite (b) in mantle-derived Cr-pyrope xenocrysts from the Internatsionalnaya kimberlite pipe, Siberian craton. Holotype samples, VII-99/1 and VII-100/1, respectively.

https://doi.org/10.1180/mgm.2023.10 Published online by Cambridge University Press

Internatsionalnaya as a whole, however, both minerals are frequently associated with other Ti- and Cr-rich oxides, i.e. rutile, picroilmenite and Cr-spinel.

After a series of preliminary studies, host pyropes were crushed and needle-like inclusions of botuobinskite and mirnyite were extracted to determine their physical and optical properties as well as to perform single-crystal X-ray examinations. Subsequently, the minerals were embedded into individual epoxy mounts for chemical analysis.

Results

Physical and optical properties

Botuobinskite and mirnyite share similar physical and optical properties; these were determined at the Fersman Mineralogical Museum, Moscow, Russia. Cleavage and parting are not observed, crystals are brittle and the fracture is uneven. Density, hardness and streak were not measured because the amount of material available for our study was limited. Using the empirical formula and unit-cell volume from single-crystal X-ray diffraction data, the calculated density is 4.3582(5) g/cm^3 for botuobinskite and 4.3867 (3) g/cm^3 for mirnyite.

Both botuobinskite and mirnyite bear a close macroscopic resemblance to other crichtonite group-members as well as to ilmenite. The examined species are opaque and jet-black in colour. In very thin slices under focused transmitted light, however, they are brown to deep cherry-red. In plane-polarised reflected light, both minerals are greyish-white with a weak brownish tint. Between crossed polars, botuobinskite and mirnyite are anisotropic in shades of bluish grey to greenish brown. No bireflectance, pleochroism, or internal reflections were observed. The reflectance values are provided in Table 1.

Chemical composition

Chemical composition of the minerals was determined by wavelength-dispersive spectrometry (WDS) using a Jeol JXA-8100 instrument at the Analytical Centre for Multi-elemental and Isotope Research, Sobolev Institute of Geology and Mineralogy (IGM SB RAS), Novosibirsk, Russia. The chemical data, probe standards and detection limits appear in Table 2. The analyses were performed with a 20 kV accelerating voltage, 100 nA sample current, a beam diameter of ~1–2 μm, and counting times of 10 s for peaks and 5–10 s for each side of the background. Raw X-ray intensities were corrected for matrix effects with a ZAF routine.

Table 1. Reflectance values*.

	Botuobinskite		Mirnyite	
Wavelength nm	R_1	R_2	R_1	R_2
400	20.2	22.8		
420	19.9	22.5		
440	19.5	20.1	22.1	24.3
460	18.9	18.9	20.3	23.7
470 (COM)	18.7	18.7	19.6	23.0
480	18.5	18.5	18.9	22.3
500	18.0	18.0	18.1	21.3
520	17.7	17.7	17.6	20.7
540	17.6	17.5	17.5	20.5
546 (COM)	17.6	17.4	17.5	20.5
560	17.5	17.3	17.6	20.6
580	17.4	17.2	17.8	20.9
589 (COM)	17.4	17.2	18.0	21.0
600	17.5	17.3	18.2	21.1
620	17.5	17.4	18.7	21.5
640	17.6	17.4	19.3	22.1
650 (COM)	17.6	17.4	19.6	22.3
660	17.6	17.4	19.8	22.4
680	17.9	17.4	20.4	22.8
700	18.2	17.5	21.2	23.4

*Measurements in air; silicon carbide used as standard; the reference wavelengths required by the Commission on Ore Mineralogy (COM) are given in bold.

The empirical formulae of botuobinskite and mirnyite calculated on the basis of 38 anions per formula unit (pfu) are as follows:

$^A(Sr_{0.26}Ba_{0.22}Ca_{0.18}La_{0.10}Ce_{0.10}K_{0.04}Na_{0.03}\square_{0.07})_{\Sigma1.00}{}^B(Fe^{2+}_{0.75}Zr_{0.22}Mn^{2+}_{0.03})_{\Sigma1.00}$
$^C(Ti_{12.33}Cr_{4.23}Fe^{3+}_{0.83}Al_{0.48}V^{3+}_{0.13})_{\Sigma18.00}{}^T(Mg_{1.59}Fe^{2+}_{0.41})_{\Sigma2.00}$
$^X(Fe_{0.48})(O_{36.98}(OH)_{1.02})_{\Sigma38.00}$ for botuobinskite and:
$^A(Sr_{0.31}Ca_{0.17}Ba_{0.15}La_{0.11}Ce_{0.11}K_{0.05}Na_{0.04}\square_{0.06})_{\Sigma1.00}{}^B(Zr_{0.61}Fe^{2+}_{0.37}Mn^{2+}_{0.02})_{\Sigma1.00}$
$^C(Ti_{12.45}Cr_{3.80}Fe^{3+}_{1.10}Al_{0.52}V^{3+}_{0.13})_{\Sigma18.00}{}^T(Mg_{1.45}Fe^{2+}_{0.55})_{\Sigma2.00}$
$^X(Fe_{0.65})O_{38}$ for mirnyite.

The ideal formula for botuobinskite is $SrFe^{2+}(Ti^{4+}_{12}Cr^{3+}_6)Mg_2[O_{36}(OH)_2]$, which requires (wt.%) SrO 6.14, FeO 4.25, TiO_2 56.76, Cr_2O_3 27.00, MgO 4.77, H_2O 1.07. For mirnyite the ideal formula is $SrZr(Ti^{4+}_{12}Cr^{3+}_6)Mg_2O_{38}$, which requires (wt.%) SrO 6.02, ZrO_2 7.16, TiO_2 55.66, Cr_2O_3 26.48, MgO 4.68.

Description of the crystal structure

Single-crystal diffraction data from botuobinskite and mirnyite crystals were measured at a STOE IPDS diffractometer equipped with a Mo X-ray tube, graphite monochromator and image plate detector. Measured frames were integrated in *CrysAlisPro* software and the *ESPERANTO* protocol was used for data transfer (Rothkirch *et al.*, 2013). The structure was solved using the *SUPERFLIP* routine (Palatinus and Chapuis, 2007) and refined in the *Jana2020* package (Petříček *et al.*, 2014). Crystal data, data collection and structure refinement details are listed in Table 3.

The solved crystal structures of botuobinskite and mirnyite both correspond to the crichtonite structural type with large 12-coordinated *A* cations, octahedral *B* and *C* sites, and tetrahedral *T* sites (Fig. 2).

Whereas large cations (Sr, Ca, Ba, La, Ce, K and Na) can be ascribed unambiguously to the 12-coordinated *A* site, the distribution of the remaining cations between the *B*, *C* and *T* sites was performed using the combination of bond-valence analysis after Chen and Adams (2017) (Table 4) and the refined electron density in the sites (Tables 5 and 6): [1] according to the bond-valence sums, Al, Cr, Ti and V should occupy only the *C* site, and Fe^{3+} contributes to the remaining electron density of this site; and [2] although bond-valence sums for Mg and Zr fit both *B* and *T* sites, the electron densities explicitly suggest that Mg resides in the *T* site with a mean atomic number of 14, and Zr in the *B* site with a mean atomic number of 21 (in botuobinskite) or 28 (in mirnyite). The remaining electron density in the *B* and *T* sites corresponds to Fe^{2+} distributed between them.

The resulting distribution of Fe between the *B*, *C*, and *T* sites generally fits the observed electron densities of the sites (Tables 5 and 6) taking into account accommodation of a certain amount of cations in additional *X* sites (see below); the bond-valence approach also allows interpreting Fe in the *C* site as trivalent and thus estimating the Fe^{3+}/Fe^{2+} ratio of the samples.

https://doi.org/10.1180/mgm.2023.10 Published online by Cambridge University Press

Table 2. Compositional data for botuobinskite and mirnyite*.

Constituent	Botuobinskite			Mirnyite			Probe standard	Detection limit (ppm)
	Mean	Range	σ	Mean	Range	σ		
Nb_2O_5	0.03	0.00–0.07	0.02	0.08	0.04–0.11	0.02	$LiNbO_3$ (synthetic)	152
TiO_2	55.80	55.64–56.26	0.32	55.45	54.05–56.16	0.54	Ilmenite	362
ZrO_2	1.52	1.44–1.58	0.04	4.20	4.10–4.38	0.07	Zircon	221
HfO_2	b.d.l.	0.00–0.16	0.05	b.d.l.	0.00–0.13	0.04	Zircon	558
Al_2O_3	1.40	1.37–1.47	0.03	1.49	1.40–1.64	0.05	Pyrope	100
V_2O_3	0.56	0.51–0.62	0.04	0.54	0.44–0.60	0.04	V_2O_5 (synthetic)	204
Cr_2O_3	18.23	18.14–18.33	0.07	16.09	15.88–16.22	0.10	Cr_2O_3 (synthetic)	142
Y_2O_3	b.d.l.	0.00–0.03	0.01	b.d.l.	0.00–0.03	0.01	$Y_3Al_5O_{12}$ (synthetic)	195
La_2O_3	0.94	0.82–1.07	0.08	1.04	0.97–1.10	0.03	$KLa(MoO_4)_2$ (synthetic)	236
Ce_2O_3	0.92	0.69–1.19	0.14	1.02	0.86–1.18	0.09	$LiCe(WO_4)_2$ (synthetic)	618
Pr_2O_3	b.d.l.	0.00–0.15	0.06	b.d.l.	0.00–0.11	0.05	$CsPr(MoO_4)_2$ (synthetic)	598
Nd_2O_3	b.d.l.	0.00–0.12	0.05	b.d.l.	0.00–0.11	0.05	$RbNd(WO_4)_2$ (synthetic)	528
MgO	3.63	3.50–3.85	0.10	3.27	3.07–3.72	0.13	Pyrope	93
CaO	0.56	0.54–0.59	0.02	0.53	0.49–0.56	0.02	Pyrope	91
MnO	0.11	0.09–0.14	0.02	0.09	0.06–0.12	0.01	Mn-rich garnet	108
FeO	4.63	9.94–10.12	0.05	4.05	10.55–10.79	0.06	Pyrope	113
Fe_2O_3**	6.03			7.35				
NiO	0.04	0.02–0.07	0.01	0.05	0.04–0.08	0.01	$NiFe_2O_4$ (synthetic)	111
SrO	1.53	1.35–1.67	0.11	1.81	1.65–2.11	0.10	Glass GL-10Sr (synthetic)	240
BaO	1.95	1.68–2.09	0.11	1.24	1.12–1.38	0.06	Glass GL-11Ba (synthetic)	394
PbO	b.d.l.	0.00–0.12	0.05	0.08	0.00–0.20	0.08	PbTe (synthetic)	543
Na_2O	0.06	0.02–0.11	0.02	0.07	0.04–0.12	0.02	Albite	111
K_2O	0.11	0.09–0.12	0.01	0.13	0.10–0.15	0.01	Orthoclase	69
H_2O_{calc}***	0.52							
Total	98.57			98.58				

*Analysis was performed using WDS on the holotype samples with: 20 kV; 100 nA; beam diameter 2 μm; $n = 14$ for botuobinskite; and $n = 18$ for mirnyite.
**The range for the analysed FeO; Fe^{3+}/Fe^{2+} is estimated taking into account that Fe is trivalent in the *C* site and divalent in the *B* and *T* sites.
***Calculated based on FTIR data.
b.d.l. – below detection limit.

Besides the *A*, *B*, *C* and *T* sites characteristic for the structural type, densely occupied in the reported structures, four additional sparsely populated octahedral sites *X*1–*X*4 were also located after a careful examination of the Fourier maps (Fig. 2). The total electron density distributed between the *X*1–*X*4 octahedral sites is ~27 electrons per formula unit for the botuobinskite structure

Table 3. Crystal data, data collection and structure refinement details.

	Botuobinskite	Mirnyite
Crystal data		
Ideal formula	$SrFe^{2+}(Ti^{4+}_{12}Cr^{3+}_{6})Mg_2[O_{36}(OH)_2]$	$SrZr(Ti^{4+}_{12}Cr^{3+}_{6})Mg_2O_{38}$
Crystal dimensions (mm)	0.1 × 0.03 × 0.03	0.1 × 0.03 × 0.03
Crystal system, space group	Trigonal, $R\bar{3}$	Trigonal, $R\bar{3}$
Temperature (K)	298	298
a, *c* (Å)	10.3644(8), 20.6588(11)	10.3734(8), 20.6910(12)
V (Å^3)	1921.9(2)	1928.2(2)
Z	3	3
Calculated density (g cm^{-3})	4.358	4.387
Data collection		
Crystal description	Black needle	Black needle
Instrument	STOE IPDS-2T	STOE IPDS-2T
Radiation type, wavelength (Å)	Mo*K*α, 0.71073	Mo*K*α, 0.71073
Number of frames	720	720
θ range (°)	2.96 to 27.55	2.95 to 27.55
Absorption correction	Empirical absorption correction using spherical harmonics	
T_{min}, T_{max}	0.474, 1	0.619, 1
No. of measured, independent and observed [$I > 2\sigma(I)$] reflections	21870, 999, 813	20600, 1001, 781
R_{int}	0.101	0.108
Data completeness to 27.55°θ (%)	100	100
Indices range of *h*, *k*, *l*	$-13 \le h \le 13$, $-13 \le k \le 13$, $-26 \le l \le 26$	$-13 \le h \le 13$, $-13 \le k \le 13$, $-26 \le l \le 24$
Refinement		
Refinement	Full-matrix least squares on F^2	Full-matrix least squares on F^2
No. of reflections, parameters, restraints	999, 116, 0	1001, 116, 0
R_1 [$I > 2\sigma(I)$], R_1(all)	0.032, 0.043	0.029, 0.044
wR_2 [$I > 2\sigma(I)$], wR_2(all)	0.061, 0.064	0.056, 0.061
GoF	1.50	1.34
$\Delta\rho_{max}$, $\Delta\rho_{min}$ (e^- Å^{-3})	1.41, −0.75	1.33, −0.58

https://doi.org/10.1180/mgm.2023.10 Published online by Cambridge University Press

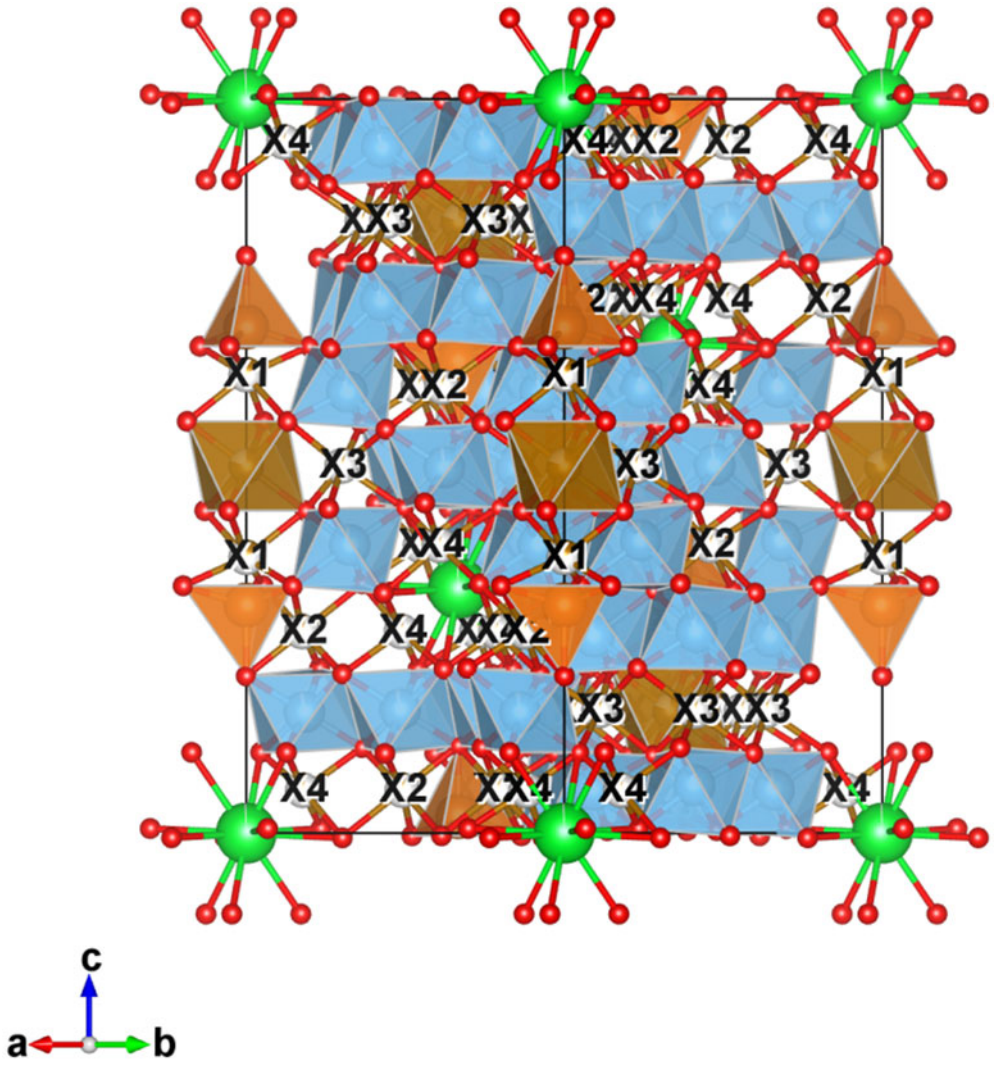

Fig. 2. Crystal structure of botuobinskite/mirnyite. 12-coordinated *A* cations are shown without their coordination polyhedra, octahedral *B* sites are shown in brown, octahedral *C* sites are shown in blue, and tetrahedral *T* sites are shown in orange. Low-populated additional octahedral sites *X*1–*X*4 are marked by corresponding symbols.

(Table 5) and 35 electrons per formula unit for the mirnyite structure (Table 6). However, one should note that side-sharing between $X1O_6$ / $X2O_6$ and TO_4 polyhedra means that the populated *X*1 and *X*2 sites are associated with vacancies in the *T* site and vice versa. Another relationship controls the *X*4 and *A* sites: the occupied *X*4 octahedral site requires the large cation

Table 4. Bond-valence sums (BVS) for cations in the *B*, *C* and *T* sites of botuobinskite and mirnyite.

	Botuobinskite							Mirnyite						
		BVS			Population, pfu				BVS			Population, pfu		
	pfu	*B*	*C*	*T*	*B*	*C*	*T*	pfu	*B*	*C*	*T*	*B*	*C*	*T*
Al^{3+}	0.48	1.6	2.5	1.8		0.48		0.52	1.7	2.5	1.8		0.52	
Cr^{3+}	4.23	2.0	3.0	2.2		4.23		3.80	2.1	3.0	2.2		3.80	
Fe^{2+}	2.47*	2.0	3.1	2.3	0.75		0.41	2.67*	2.1	3.1	2.2	0.37		0.55
Fe^{3+}		2.2	3.3	2.4		0.83			2.3	3.3	2.4		1.10	
Mg^{2+}	1.59	1.8	2.8	2.0			1.59	1.45	1.9	2.8	2.0			1.45
Mn^{2+}	0.03	2.4	3.6	2.7	0.03			0.02	2.5	3.6	2.6	0.02		
Ti^{4+}	12.33	2.5	3.9	2.8		12.33		12.45	2.6	3.8	2.8		12.45	
V^{3+}	0.13	2.1	3.2	2.3		0.13		0.13	2.2	3.2	2.3		0.13	
Zr^{4+}	0.22	3.5	5.4	4.0	0.22			0.61	3.7	5.3	3.9	0.61		
avg. BVS**		2.3	3.6	2.1					3.1	3.6	2.1			

*The excess of Fe (0.48 pfu for botuobinskite and 0.65 for mirnyite) is attributed to the *X* sites.
**Calculated based on the ascribed site occupancies.

https://doi.org/10.1180/mgm.2023.10 Published online by Cambridge University Press

Table 5. Distribution of cations between crystallographic positions of botuobinskite.

Site	M.a.n.	*N* pfu	Site scattering observed (epfu)	Ascribed site populations (pfu)	Site scattering calculated (epfu)
A	37.66	1	37.66	$Sr_{0.26}Ba_{0.22}Ca_{0.18}La_{0.10}Ce_{0.10}K_{0.04}Na_{0.03}\square_{0.07}$	38.06
B	20.75	1	20.75	$Fe_{0.75}Zr_{0.22}Mn_{0.03}$	29.05
*C*1 + *C*2 + *C*3	20.55	18	369.86	$Ti_{12.33}Cr_{4.23}Fe_{0.83}Al_{0.48}V_{0.13}$	403.59
T	13.96	2	27.91	$Mg_{1.59}Fe_{0.41}$	29.74
*X*1 + *X*2 + *X*3 + *X*4			26.68	$Fe_{0.48}$	12.48
Σ			482.86		512.92

M.a.n. – mean atomic number; epfu – electrons per formula unit.

Table 6. Distribution of cations between crystallographic positions of mirnyite.

Site	M.a.n.	*N* pfu	Site scattering observed (epfu)	Ascribed site populations (pfu)	Site scattering calculated (epfu)
A	33.33	1	33.33	$Sr_{0.31}Ca_{0.17}Ba_{0.15}La_{0.11}Ce_{0.11}K_{0.05}Na_{0.04}\square_{0.06}$	37.62
B	28.16	1	28.16	$Zr_{0.61}Fe_{0.37}Mn_{0.02}$	34.52
*C*1 + *C*2 + *C*3	20.06	18	361.02	$Ti_{12.45}Cr_{3.80}Fe_{1.10}Al_{0.52}V_{0.13}$	403.45
T	13.80	2	27.60	$Mg_{1.45}Fe_{0.55}$	31.70
*X*1 + *X*2 + *X*3 + *X*4			35.45	$Fe_{0.65}$	16.90
Σ			485.56		524.19

M.a.n. – mean atomic number; epfu – electrons per formula unit.

Table 7. Correspondence between the *X*1–*X*4 sites and previously reported low-occupied cation sites in the crichtonite-group members.

Site	e^- per site, botuobinskite	e^- per site, mirnyite	Gatehouse *et al.* (1983)	Armbruster and Kunz (1990)	Orlandi *et al.* (1997)	Biagioni *et al.* (2014)
*X*1 (6c)	3.7	3.8	M6	M6	M6	M8
*X*2 (18*f*)	1.1	1.5		M9	M8	M6
*X*3 (18*f*)	1.1	1.7		M7	M7	M7
*X*4 (18*f*)	0.9	1.4		M8	(M9)	(M9)

A site to be populated by an oxygen anion. The correspondence between the *X*1–*X*4 sites and previously reported low-occupation cation sites in the crichtonite-group members is summarised in Table 7.

Fractional atomic coordinates and isotropic or equivalent isotropic displacement parameters for botuobinskite and mirnyite are presented in Tables 8 and 9, respectively, whereas bond lengths appear in Tables 10 and 11. The crystallographic information files have been deposited with the Principal Editor of *Mineralogical Magazine* and are available as Supplementary material (see below).

Table 8. Fractional atomic coordinates and isotropic or equivalent isotropic displacement parameters (Å^2) for botuobinskite. Effective occupancies correspond to dominant cation (Sr, Fe, Ti, Mg and Fe for the *A*–*X* sites, respectively).

	Occupancy	*x*	*y*	*z*	U_{iso}*/U_{eq}
A	0.991(7)	0	0	0	0.0188(3)
B	0.798(7)	⅓	⅔	⅙	0.0191(6)
*C*1	0.959(6)	–0.19444(7)	0.28944(7)	0.16841(3)	0.0120(3)
*C*2	0.923(6)	0.09281(8)	0.35030(7)	0.26794(3)	0.0128(3)
*C*3	0.920(6)	0.00792(8)	0.58482(8)	0.27414(3)	0.0143(3)
T	1.163(12)	0	0	0.31050(8)	0.0110(6)
O1		0.1479(3)	0.5364(3)	0.22745(12)	0.0168(11)
O2		0.2308(2)	0.3047(2)	0.22471(11)	0.0124(10)
O3		–⅓	⅓	0.1193(2)	0.0135(12)
O4		–0.1616(3)	0.4598(2)	0.22328(12)	0.0138(10)
O5		–0.0751(3)	0.2275(3)	0.21681(12)	0.0135(10)
O6		–0.0315(3)	0.4004(3)	0.32701(12)	0.0158(11)
O7		0.0525(3)	0.1984(3)	0.33689(12)	0.0158(11)
*X*1	0.141(4)	0	0	0.3756(3)	0.019(2)*
*X*2	0.044(2)	0.1761(11)	0.1246(11)	0.2746(5)	0.005(4)*
*X*3	0.044(3)	0.1095(12)	0.3652(12)	0.1670(5)	0.011(4)*
*X*4	0.036(3)	–0.2742(13)	0.5114(13)	0.2747(6)	0.006(5)*

Raman spectroscopy

Both botuobinskite and mirnyite are isostructural with other crichtonite-group minerals and crystallise in the $R\bar{3}$ space group. Thus, based on the crystallography and crystal structure refinement parameters the fundamental phonons at the Γ point (i.e. Brillouin zone centre) can be represented by factor-group analysis (using the Bilbao Crystallographic Server, Kroumova *et al.*, 2003) as follows:

$$\Gamma\text{optic} = 30A_g\ (R) + 31A_u\ (IR) + 30^1E_g\ (R) + 31^1E_u\ (IR) + 30^2E_g\ (R) + 31^2E_u\ (IR),$$

where R and IR are Raman-active and infrared-active modes, respectively. Due to the centre of symmetry in the rhombohedral unit cell, all the phonons that are infrared appear as forbidden for Raman, and vice versa (Porto *et al.*, 1967).

The Raman spectra of the minerals are shown in Fig. 3. The spectra were obtained with a Horiba Jobin Yvon LabRam HR 800 mm spectrometer coupled with a Nd:YAG 532 nm excitation wavelength

https://doi.org/10.1180/mgm.2023.10 Published online by Cambridge University Press

Table 9. Fractional atomic coordinates and isotropic or equivalent isotropic displacement parameters (Å^2) for mirnyite. Effective occupancies correspond to dominant cation (Sr, Zr, Ti, Mg and Fe for the *A*–*X* sites, respectively).

	Occupancy	*x*	*y*	*z*	U_{iso}*/U_{eq}
A	0.877(6)	0	0	0	0.0192(3)
B	0.704(5)	⅓	⅔	⅙	0.0189(4)
*C*1	0.936(6)	−0.04339(7)	0.81722(7)	0.16486(3)	0.0121(3)
*C*2	0.901(6)	0.01658(7)	0.59049(7)	0.06538(3)	0.0117(3)
*C*3	0.898(5)	0.25149(7)	0.91081(8)	0.05902(3)	0.0133(3)
T	1.150(11)	−⅓	⅓	0.02297(8)	0.0103(5)
O1		0.1265(2)	0.9547(2)	0.10985(11)	0.0148(10)
O2		0.2044(2)	0.7214(2)	0.10599(11)	0.0165(10)
O3		−0.0286(2)	0.4077(2)	0.10852(11)	0.0125(9)
O4		−0.1349(3)	0.4794(3)	−0.00303(11)	0.0155(10)
O5		0	1	0.21434(19)	0.0135(11)
O6		−0.1060(2)	0.6358(2)	0.11632(11)	0.0136(10)
O7		0.0674(3)	0.7652(2)	0.00644(11)	0.0160(10)
*X*1	0.096(3)	−⅓	⅓	−0.0425(3)	0.026(2)*
*X*2	0.0372(17)	−0.5104(9)	0.2084(9)	0.0589(4)	0.012(3)*
*X*3	0.0420(17)	0.0302(10)	0.5883(11)	0.1658(4)	0.027(3)*
*X*4	0.0365(19)	0.1778(11)	1.1190(11)	0.0589(5)	0.020(4)*

Table 10. Bond lengths (Å) for botuobinskite.

A–O4	2.779 (3) ×6	*C*1–O2	1.968 (2)	*C*2–O1	1.909 (3)
A–O6	2.848 (4) ×6	*C*1–O3	1.991 (2)	*C*2–O2	1.934 (3)
		*C*1–O4	1.979 (3)	*C*2–O5	1.884 (2)
B–O1	2.121 (3) ×6	*C*1–O4	2.038 (3)	*C*2–O6	2.021 (3)
		*C*1–O5	1.933 (3)	*C*2–O7	2.006 (3)
*C*3–O1	2.004 (3)	*C*1–O5	1.988 (3)	*C*2–O7	2.131 (2)
*C*3–O2	1.964 (3)				
*C*3–O4	1.896 (2)	*T*–O3	1.993 (4)		
*C*3–O6	2.058 (3)	*T*–O7	1.924 (4) ×3		
*C*3–O6	1.974 (4)				
*C*3–O7	2.033 (3)				

laser and an Olympus BX41 microscope at IGM SB RAS. Further analytical details were provided by Alifirova *et al.* (2020).

The Raman peaks are located in the region 80–1000 cm^{-1}. According to the factor-group analysis, the influence on the Raman spectra comes from phonon modes related to the 6*c* and 18*f* Wyckoff positions. In the unit cell they refer to the motions within *M*2 tetrahedral (*T*) and *M*3–*M*5 octahedral (*C*) units (i.e. internal modes) as well as to the rotations and translations of those entire units (i.e. external modes). The *A* and *B* positions have no impact on the Raman spectra. The phonon modes predicted above are located at 133, 187, 313, 409–411, 711 and 809 cm^{-1} (Fig. 3). The Raman modes can be revealed mostly by means of the Raman spectrum fitting procedure. The spectral bands in the O–H stretching region are expected to be inactive for Raman and do not occur in the obtained spectra at chosen parameters. Further assignment of theoretically predicted Γ point phonons was not made for this study.

Table 11. Bond lengths (Å) for mirnyite.

A–O1	2.780 (3) ×6	*C*1–O1	1.981 (2)	*C*2–O2	1.924 (2)
A–O7	2.854 (4) ×6	*C*1–O1	2.047 (4)	*C*2–O3	1.930 (3)
		*C*1–O3	1.969 (3)	*C*2–O4	1.997 (2)
B–O2	2.109 (3) ×6	*C*1–O5	1.998 (2)	*C*2–O4	2.141 (3)
		*C*1–O6	1.936 (3)	*C*2–O6	1.883 (3)
*C*3–O1	1.893 (3)	*C*1–O6	1.994 (2)	*C*2–O7	2.023 (3)
*C*3–O2	2.021 (3)				
*C*3–O3	1.968 (3)	*T*–O4	1.925 (4) ×3		
*C*3–O4	2.041 (4)	*T*–O5	1.987 (4)		
*C*3–O7	2.056 (2)				
*C*3–O7	1.974 (3)				

The comprehensive Raman data on botuobinskite and other crichtonite-group minerals included in mantle garnets from a suite of Siberian kimberlites and lamprophyres were reported in (Alifirova *et al.*, 2020).

Fourier-transform infrared spectroscopy (FTIR)

A piece of the largest botuobinskite grain (Fig. 1) was polished from both sides to get a 50 μm thick plate. The spectra were recorded in air at room temperature using a Bruker Vertex 70 spectrometer equipped with a Hyperion 2000 infrared (IR) microscope at IGM SB RAS. IR spectroscopy data were acquired in a wavelength range of 7000–600 cm^{-1}, with a resolution 2–4 cm^{-1}, 30–70 scans and a 50 × 50 μm aperture.

The absorption bands corresponding to O–H bond vibrations are observed within the ~3750–3100 cm^{-1} and ~1650–1400 cm^{-1} wavelength regions (Fig. 4). A broad absorption band in the former region is characteristic of the H–O stretching of the hydroxyl groups, showing strong bands at 3703 and 3660 cm^{-1} as well as shoulders at 3570 and 3420 cm^{-1}. Minor weak bands at 1610 and 1510 cm^{-1} may be attributed to the metal–O–H overtones and to H–O–H bending, respectively. The amount of water was calculated following the Beer–Lambert law $A = \epsilon \cdot t \cdot c$, where A is absorbance, ϵ is the molar absorption coefficient, t is the plate thickness and c is the concentration of the absorbing species in the sample. The integrated absorbance values (band areas) and the integrated molar absorption coefficient obtained by the calibration of the Libowitzky and Rossman (1997) were used in the equation. The calculated amount of water is 0.52 wt.% H_2O, which corresponds to 1.02 OH^- pfu.

Discussion

Relationship to other mineral species of the crichtonite group

Comparative data for the new minerals and related species of the crichtonite group in terms of site occupancies are given in Table 12. Both minerals exhibit compositional similarities to other crichtonite-group species occurring in the lithospheric mantle (i.e. loveringite, lindsleyite and mathiasite). Mirnyite may be considered as a Sr-dominant (in the *A* site) analogue of these mantle-derived species, whereas botuobinskite shows *A*- and *B*-site occupancies different from other mantle crichtonites.

Alternatively, both botuobinskite and mirnyite can be considered as analogues of other Sr-dominant crichtonite-group minerals that are of crustal origin, such as crichtonite (*sensu stricto*), dessauite-(Y), mapiquiroite and saranovskite, yet showing different *B*- and *T*-site occupancy as well as characteristic enrichment in magnesium and chromium.

Review of botuobinskite and mirnyite occurrences

From the available literature data, one may trace a few other occurrences of botuobinskite and mirnyite in samples derived from the subcontinental lithospheric mantle. Botuobinskite and mirnyite appear to be relatively abundant as mineral inclusions in Cr-rich peridotitic garnets worldwide. More specifically, a mineral with a composition corresponding to botuobinskite was reported in a Cr-pyrope xenocryst from the Zagadochnaya

https://doi.org/10.1180/mgm.2023.10 Published online by Cambridge University Press

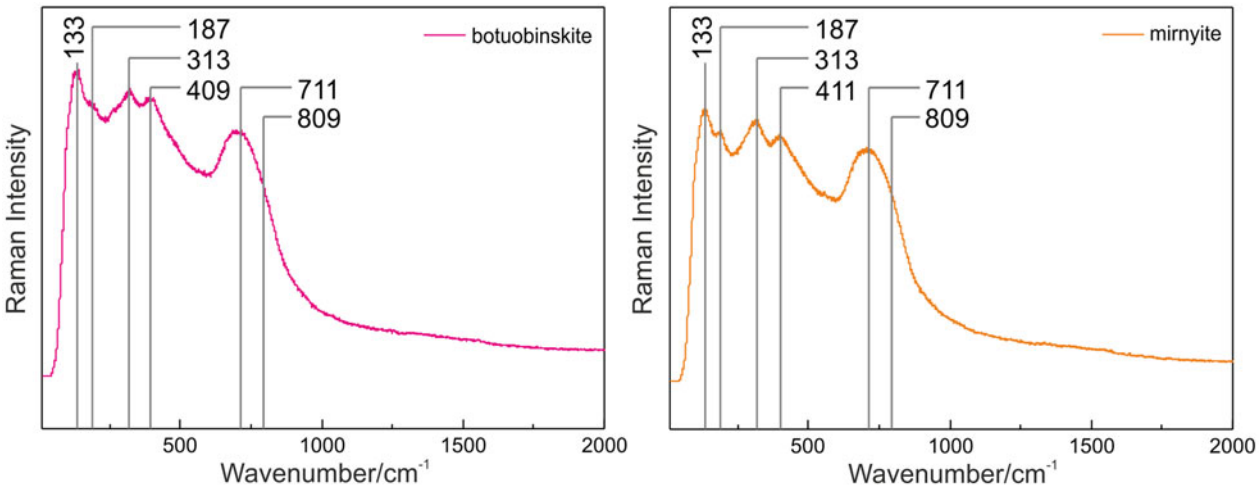

Fig. 3. Raman spectra of botuobinskite (left) and mirnyite (right).

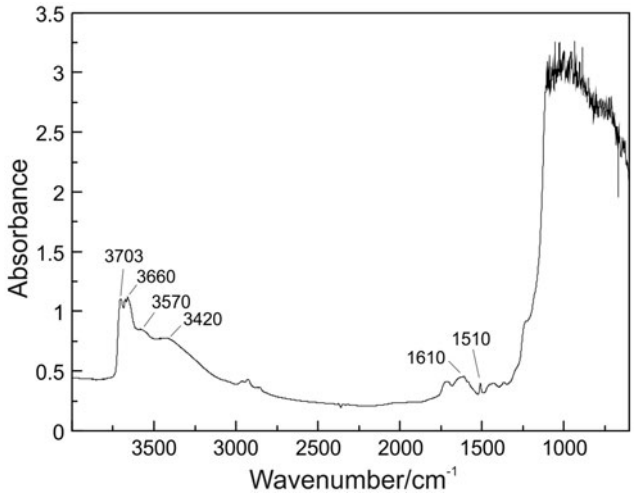

Fig. 4. Infrared spectrum of botuobinskite.

kimberlite (Ziberna *et al.*, 2013). Both minerals have been documented in pyrope crystals from an ultramafic diatreme of the Garnet Ridge cluster, Arizona, USA (Wang *et al.*, 1999). Botuobinskite has also been recognised in composite polymineralic inclusions in Cr-pyrope crystals from the Aldanskaya lamprophyre dyke, Chompolo field, southeastern Siberian craton (Rezvukhin *et al.*, 2022). Apart from the findings in intimate association with pyrope, mirnyite occasionally occurs in association with the typical LIMA series (lindsleyite–mathiasite solid solution) Zr-enriched titanates in metasomatised peridotite xenoliths sampled by South African kimberlites (Haggerty *et al.*, 1983; Haggerty, 1991; Gregoire *et al.*, 2002; Konzett *et al.*, 2013).

Implications for mantle metasomatic processes

Crichtonite-group titanates are important repositories of incompatible elements within the subcontinental lithospheric mantle.

Table 12. Crichtonite-group minerals approved by IMA–CNMNC and their structural formula.

Mineral	*M*0 (^{XII}A)	*M*1 (^{VI}B)	*M*2 (^{IV}T)	*M*3–*M*5 (^{VI}C)	Φ*	References
Crichtonite	Sr	(Mn, Y, U)	Fe_2	$(Ti, Fe, Cr, V)_{18}$	$(O, OH)_{38}$	[1]
Senaite	Pb	(Mn, Y, U)	$(Fe, Zn)_2$	$(Ti, Fe, Cr, V)_{18}$	$(O, OH)_{38}$	[2], [3]
Davidite-(La)	La	(Y, U)	Fe_2	$(Ti, Fe, Cr, V)_{18}$	$(O, OH, F)_{38}$	[4]
Davidite-(Ce)	Ce	(Y, U)	Fe_2	$(Ti, Fe, Cr, V)_{18}$	$(O, OH, F)_{38}$	[4]
Landauite	(Na, Pb)	(Mn^{2+}, Y)	$(Zn, Fe)_2$	$(Ti, Fe^{3+}, Nb)_{18}$	$(O, OH, F)_{38}$	[5]
Dessauite-(Y)	Sr	(Y, U, Mn)	Fe_2	$(Ti, Fe, Cr, V)_{18}$	$(O, OH)_{38}$	[6]
Gramaccioliite-(Y)	(Pb, Sr)	(Y, Mn)	Fe_2^{3+}	$(Ti, Fe^{3+})_{18}$	O_{38}	[7]
Cleusonite	Pb	(U^{4+}, U^{6+})	Fe_2^{2+}	$(Ti, Fe^{2+}, Fe^{3+})_{18}$	$(O, OH)_{38}$	[8]
Paseroite	Pb	$(Mn^{2+}, □)$	$(Fe^{3+}, □)_2$	$(V^{5+}, Ti^{4+}, □)_{18}$	O_{38}	[9]
Mapiquiroite	(Sr, Pb)	(U, Y)	Fe_2	$(Ti, Fe^{3+})_{18}$	O_{38}	[10]
Almeidaite	Pb	(Mn, Y)	Zn_2	$(Ti, Fe^{3+})_{18}$	$O_{36}(OH,O)_2$	[11]
Mianningite	(□, Pb, Ce, Na)	(U^{4+}, Mn, U^{6+})	Fe_2^{3+}	$(Ti, Fe^{3+})_{18}$	O_{38}	[12]
Loveringite	(Ca, Ce, La)	(Zr, Fe)	$(Mg, Fe)_2$	$(Ti, Fe, Cr, Al)_{18}$	O_{38}	[13], [14]
Lindsleyite	(Ba, Sr)	(Zr, Ca)	$(Mg, Fe)_2$	$(Ti, Cr, Fe)_{18}$	O_{38}	[15]
Mathiasite	(K, Ba, Sr)	(Zr, Fe)	$(Mg, Fe)_2$	$(Ti, Cr, Fe)_{18}$	O_{38}	[15], [16]
Saranovskite	(Sr, Ba, Ce, Ca)	(Ca, Y, Fe, Zr, Ce, Mn)	$(Fe, Mg)_2$	$(Ti, Cr, Fe^{2+}, Fe^{3+}, Al, Sc)_{18}$	O_{38}	[17]
Haitaite-(La)	La	U^{4+}	Fe_2^{3+}	$(Ti, Fe^{2+}, Fe^{3+})_{18}$	O_{38}	[18]
Botuobinskite	(Sr, Ba, Ca)	(Fe, Zr)	$(Mg, Fe)_2$	$(Ti, Cr, Fe, Al)_{18}$	$(O, OH)_{38}$	[19]
Mirnyite	(Sr, Ca, Ba)	(Zr, Fe)	$(Mg, Fe)_2$	$(Ti, Cr, Fe, Al)_{18}$	O_{38}	[19]

Data are from the IMA List of Minerals, updated in November 2022 (Pasero, 2022). *Φ = 38 for all members of the crichtonite group. Possible additional cations in octahedral sites (Armbruster and Kunz, 1990; Gatehouse *et al.*, 1983; Orlandi *et al.*, 1997) are not considered.

Key references: [1] Grey *et al.* (1976); [2] Grey and Lloyd (1976); [3] Armbruster and Kunz (1990); [4]Gatehouse *et al.* (1979); [5] Grey and Gatehouse (1978); [6] Orlandi *et al.* (1997); [7] Orlandi *et al.* (2004); [8] Wülser *et al.* (2005); [9] Mills *et al.* (2012); [10] Biagioni *et al.* (2014); [11] Menezes *et al.* (2015); [12] Ge *et al.* (2017); [13] Gatehouse *et al.* (1978); [14] Kelly *et al.* (1979); [15] Haggerty *et al.* (1983); [16] Gatehouse *et al.* (1983); [17] Chukanov *et al.* (2020); [18] Wang *et al.* (2021); [19] this study.

https://doi.org/10.1180/mgm.2023.10 Published online by Cambridge University Press

As estimated by Jones (1989), "approximately 1 part in 1000 titanate, occurring as discrete grains or grain boundary phases, would double the content of Ba, LREE (La, Ce), Rb, Sr, and U in average mantle". The Sr-specific mineral species of the crichtonite group (i.e. botuobinskite and mirnyite) are particularly notable for their association with Cr-pyrope of lherzolitic paragenesis in the lithospheric mantle assemblages (e.g. Wang *et al.*, 1999; Rezvukhin *et al.*, 2018, 2022). To the best of our knowledge, crichtonite-group titanates have never been documented in association with depleted harzburgitic or dunitic garnet. These minerals are thus indicative of lherzolite-producing metasomatism (refertilisation) that is accepted to be a widespread phenomenon in the lithospheric mantle of ancient cratons (e.g. Stachel *et al.*, 2004; Malkovets *et al.*, 2007; O'Reilly and Griffin, 2013). The crichtonite-group minerals probably exert a strong control on the trace-element partitioning during refertilisation, although numerical modelling is currently lacking. During the metasomatic harzburgite-to-lherzolite transition Sr and LREE partition strongly into newly-formed clinopyroxene (e.g. Griffin *et al.*, 1999b). In this regard, it is probably important that the crichtonite-group minerals that frequently accompany pyrope and clinopyroxene in lherzolites represent previously overlooked (yet significant) components that effectively scavenge Sr and LREE as well.

The diversity of incompatible elements that may occupy positions *A* and *B* makes mantle-derived crichtonite-group titanates a potential tool for deciphering the processes of metasomatism in the lithospheric mantle of ancient cratons as well as for reconstructing the composition of the metasomatic agents (melt or fluids). In particular, the mantle-derived pyrope-hosted crichtonite-group titanates from the Internatsionalnaya kimberlite pipe are characterised by compositions rich in Na, Ca, Sr and REE, whereas those from South African kimberlites (LIMA series) are mostly Ba and K rich. The former also have larger Al contents than the latter, which probably reflects equilibrium with the host garnet (Rezvukhin *et al.*, 2018, 2022). These differences indicate that the compositions of the metasomatic melts or fluids circulating in the lithospheric mantle of the Siberian and Kaapvaal cratons were not identical.

The crichtonite group currently comprises 19 mineral species, of which seven have been discovered over the last ten years. The diverse range of mineral compositions of known crichtonite-group species (Table 12) and the existence of a plethora of structural positions for isomorphic substitutions promise new systematic discoveries within this mineral group in the future.

Acknowledgements. SEM-EDS examinations, crystal data collection and structure refinement studies were supported by the Russian Science Foundation project No. 18-77-10062-P (https://rscf.ru/en/project/21-77-03004/). Electron microprobe WDS analyses were performed within the Russian Science Foundation project No. 18-17-00249. Sample preparation, Raman and FTIR studies were carried out within the state assignment project of IGM SB RAS.

We thank Dmitriy Belakovskiy (Fersman Mineralogical Museum, Moscow) for fruitful discussions and help in determining physical properties of the minerals. We are also grateful to Yurii Kupriyanov (IGM SB RAS) who assisted with FTIR analyses of botuobinskite. Thanks are extended to William L. Griffin (Macquarie University, Sydney) for editing English. Journal Editors Stuart Mills and Helen Kerbey provided efficient editorial handling. The manuscript benefited from the comments of Stuart Mills and three anonymous reviewers.

Supplementary material. To view supplementary material for this article, please visit https://doi.org/10.1180/mgm.2023.10

Competing interests. The authors declare none.

References

Agashev A.M., Nakai S.i., Serov I.V., Tolstov A.V., Garanin K.V. and Kovalchuk O.E. (2018) Geochemistry and origin of the Mirny field kimberlites, Siberia. *Mineralogy and Petrology*, **112**, 597–608.

Alifirova T., Rezvukhin D., Nikolenko E., Pokhilenko L., Zelenovskiy P., Sharygin I., Korsakov A. and Shur V. (2020) Micro-Raman study of crichtonite group minerals enclosed into mantle garnet. *Journal of Raman Spectroscopy*, **51**, 1493–1512.

Armbruster T. and Kunz M. (1990) Cation arrangement in a unusual uranium-rich senaite: crystal structure study at 130 K. *European Journal of Mineralogy*, **2**, 163–170.

Biagioni C., Orlandi P., Pasero M., Nestola F. and Bindi L. (2014) Mapiquiroite, $(Sr,Pb)(U,Y)Fe_2(Ti,Fe^{3+})_{18}O_{38}$, a new member of the crichtonite group from the Apuan Alps, Tuscany, Italy. *European Journal of Mineralogy*, **26**, 427–437.

Chen H. and Adams S. (2017) Bond softness sensitive bond-valence parameters for crystal structure plausibility tests. *IUCrJ*, **4**, 614–625.

Chukanov N.V., Rastsvetaeva R.K., Kazheva O.N., Ivanov O.K., Pekov I.V., Agakhanov A.A., Van K.V., Shcherbakov V.D. and Britvin S.N. (2020) Saranovskite, $SrCaFe_2^{2+}(Cr_4Ti_2)Ti_{12}O_{38}$, a new crichtonite-group mineral. *Physics and Chemistry of Minerals*, **47**, 1–11.

Gatehouse B.M., Grey I.E., Campbell I.H. and Kelly P. (1978) The crystal structure of loveringite – a new member of the crichtonite group. *American Mineralogist*, **63**, 28–36.

Gatehouse B.M., Grey I.E. and Kelly P.R. (1979) The crystal structure of davidite. *American Mineralogist*, **64**, 1010–1017.

Gatehouse B.M., Grey I.E. and Smyth J.R. (1983) Structure refinement of mathiasite, $(K_{0.62}Na_{0.14}Ba_{0.14}Sr_{0.10})_{\Sigma 1.0}[Ti_{12.90}Cr_{3.10}Mg_{1.53}Fe_{2.15}Zr_{0.67}Ca_{0.29}(V,Nb,Al)_{0.36}]\Sigma_{21.0}O_{38}$. *Acta Crystallographica*, **C39**, 421–422.

Ge X., Fan G., Li G., Shen G., Chen Z. and Ai Y. (2017) Mianningite, $(\square,Pb,Ce,Na)(U^{4+},Mn,U^{6+})Fe_2^{3+}(Ti,Fe^{3+})_{18}O_{38}$, a new member of the crichtonite group from Maoniuping REE deposit, Mianning county, southwest Sichuan, China. *European Journal of Mineralogy*, **29**, 331–338.

Gregoire M., Bell D.R. and Le Roex A.P. (2002) Trace element geochemistry of phlogopite-rich mafic mantle xenoliths: their classification and their relationship to phlogopite-bearing peridotites and kimberlites revisited. *Contributions to Mineralogy and Petrology*, **142**, 603–625.

Grey I.E. and Gatehouse B.M. (1978) The crystal structure of landauite, $Na[MnZn_2(Ti,Fe)_6Ti_{12})]O_{38}$. *The Canadian Mineralogist*, **16**, 63–68.

Grey I.E. and Lloyd D.J. (1976) The crystal structure of senaite. *Acta Crystallographica*, **B32**, 1509–1513.

Grey I.E., Lloyd D.J. and White J.S. (1976) The structure of crichtonite and its relationship to senaite. *American Mineralogist*, **61**, 1203–1212.

Griffin W.L., Ryan C.G., Kaminsky F.V., O'Reilly S.Y., Natapov L.M., Win T.T., Kinny P.D. and Ilupin I.P. (1999a) The Siberian lithosphere traverse: mantle terranes and the assembly of the Siberian Craton. *Tectonophysics*, **310**, 1–35.

Griffin W.L., Shee S.R., Ryan C.G., Win T.T. and Wyatt B.A. (1999b) Harzburgite to lherzolite and back again: metasomatic processes in ultramafic xenoliths from the Wesselton kimberlite, Kimberley, South Africa. *Contributions to Mineralogy and Petrology*, **134**, 232–250.

Haggerty S.E. (1991) Oxide mineralogy of the upper mantle. Pp. 355–416 in: *Oxide Minerals: Petrologic and Magnetic Significance* (D.H. Lindsley, editor). Reviews in Mineralogy, 25. Mineralogical Society of America, Washington DC.

Haggerty S.E., Smyth J.R., Erlank A.J., Rickard R.S. and Danchin R.V. (1983) Lindsleyite (Ba) and mathiasite (K): two new chromium-titanates in the crichtonite series from the upper mantle. *American Mineralogist*, **68**, 494–505.

Jones A.P. (1989) Upper-mantle enrichment by kimberlitic or carbonatitic magmatism. Pp. 448–463 in: *Carbonatites* (K. Bell, editors). Unwin Hyman, London.

Kelly P.R., Campbell I.H., Grey I.E. and Gatehouse B.M. (1979) Additional data on loveringite $(Ca,REE)(Ti,Fe,Cr)_{21}O_{38}$ and mohsite discredited. *The Canadian Mineralogist*, **17**, 635–638.

Kiselev A., Yarmolyuk V., Ivanov A. and Egorov K. (2014) Middle Paleozoic basaltic and kimberlitic magmatism in the northwestern shoulder of the Vilyui Rift, Siberia: relations in space and time. *Russian Geology and Geophysics*, **55**, 144–152.

Konzett J., Wirth R., Hauzenberger C. and Whitehouse M. (2013) Two episodes of fluid migration in the Kaapvaal Craton lithospheric mantle associated with Cretaceous kimberlite activity: evidence from a harzburgite containing a unique assemblage of metasomatic zirconium-phases. *Lithos*, **182–183**, 165–184.

Kroumova E., Aroyo M.I., Perez-Mato J.M., Kirov A., Capillas C., Ivantchev S. and Wondratschek H. (2003) Bilbao Crystallographic Server: Useful Databases and Tools for Phase-Transition Studies. *Phase Transitions*, **76**, 155–170.

Libowitzky E. and Rossman G.R. (1997) An IR absorption calibration for water in minerals. *American Mineralogist*, **82**, 1111–1115.

Malkovets V.G., Griffin W.L., O'Reilly S.Y. and Wood B.J. (2007) Diamond, subcalcic garnet, and mantle metasomatism: Kimberlite sampling patterns define the link. *Geology*, **35**, 339–342.

Malkovets V.G., Rezvukhin D.I., Belousova E.A., Griffin W.L., Sharygin I.S., Tretiakova I.G., Gibsher A.A., O'Reilly S.Y., Kuzmin D.V., Litasov K.D., Logvinova A.M., Pokhilenko N.P. and Sobolev N.V. (2016) Cr-rich rutile: A powerful tool for diamond exploration. *Lithos*, **265**, 304–311.

Menezes F.L.A.D., Chukanov N.V., Rastsvetaeva R.K., Aksenov S.M., Pekov I.V., Chaves M.L.S.C., Richards R.P., Atencio D., Brandão P.R.G., Scholz R., Krambrock K., Moreira R.L., Guimaraes F.S., Romano A.W., Persiano A.C., Oliveira L.C.A. and Ardisson J.D. (2015) Almeidaite, Pb(Mn,Y)$Zn_2(Ti,Fe^{3+})_{18}O_{36}(O,OH)_2$, a new crichtonite-group mineral, from Novo Horizonte, Bahia, Brazil. *Mineralogical Magazine*, **79**, 269–283.

Mills S.J., Bindi L., Cadoni M., Kampf A.R., Ciriotti M.E. and Ferraris G. (2012) Paseroite, $PbMn^{2+}(Mn^{2+},Fe^{2+})_2(V^{5+},Ti,Fe^{3+},\square)_{18}O_{38}$, a new member of the crichtonite group. *European Journal of Mineralogy*, **24**, 1061–1067.

O'Reilly S.Y. and Griffin W.L. (2013) Mantle metasomatism. Pp. 471–533 in: *Metasomatism and the Chemical Transformation of Rock*. Springer, Berlin–Heidelberg.

Orlandi P., Pasero M., Duchi G. and Olmi F. (1997) Dessauite, (Sr,Pb)(Y,U)$(Ti,Fe^{3+})_{20}O_{38}$, a new mineral of the crichtonite group from Buca della Vena mine, Tuscany, Italy. *American Mineralogist*, **82**, 807–811.

Orlandi P., Pasero M., Rotiroti N., Filippo O., Demartin F. and Moëlo Y. (2004) Gramaccioliite-(Y), a new mineral of the crichtonite group from Stura Valley, Piedmont, Italy. *European Journal of Mineralogy*, **16**, 171–175.

Palatinus L. and Chapuis G. (2007) SUPERFLIP – a computer program for the solution of crystal structures by charge flipping in arbitrary dimensions. *Journal of Applied Crystallography*, **40**, 786–790.

Pasero M. (2022) The New IMA List of Minerals. International Mineralogical Association. Commission on new minerals, nomenclature and classification (IMA-CNMNC). http://cnmnc.main.jp/.

Petříček V., Dušek M. and Palatinus L. (2014) Crystallographic computing system JANA2006: general features. *Zeitschrift für Kristallographie-Crystalline Materials*, **229**, 345–352.

Porto S.P.S. and Krishnan R.S. (1967) Raman effect of corundum. *The Journal of Chemical Physics*, **47**, 1009–1012.

Rezvukhin D.I., Malkovets V.G., Sharygin I.S., Kuzmin D.V., Gibsher A.A., Litasov K.D., Pokhilenko N.P. and Sobolev N.V. (2016a) Inclusions of crichtonite group minerals in pyropes from the Internatsionalnaya kimberlite pipe, Yakutia. *Doklady Earth Sciences*, **466**, 206–209.

Rezvukhin D.I., Malkovets V.G., Sharygin I.S., Kuzmin D.V., Litasov K.D., Gibsher A.A., Pokhilenko N.P. and Sobolev N.V. (2016b) Inclusions of Cr-and Cr–Nb-Rutile in pyropes from the Internatsionalnaya kimberlite pipe, Yakutia. *Doklady Earth Sciences*, **466**, 173–176.

Rezvukhin D.I., Malkovets V.G., Sharygin I.S., Tretiakova I.G., Griffin W.L. and O'Reilly S.Y. (2018) Inclusions of crichtonite-group minerals in Cr-pyropes from the Internatsionalnaya kimberlite pipe, Siberian Craton: Crystal chemistry, parageneses and relationships to mantle metasomatism. *Lithos*, **308–309**, 181–195.

Rezvukhin D.I., Rashchenko S.V., Sharygin I.S., Malkovets V.G., Alifirova T.A., Pautov L.A., Nigmatulina E.N. and Seryotkin Y.V. (2020a) Botuobinskite, IMA 2018-143a. CNMNC Newsletter No. 57. *Mineralogical Magazine*, **84**, 791–794, https://doi.org/10.1180/mgm.2020.73

Rezvukhin D.I., Rashchenko S.V., Sharygin I.S., Malkovets V.G., Alifirova T.A., Pautov L.A., Nigmatulina E.N. and Seryotkin Y.V. (2020b) Mirnyite, IMA 2018-144a. CNMNC Newsletter No. 57. *Mineralogical Magazine*, **84**, 791–794, https://doi.org/10.1180/mgm.2020.73

Rezvukhin D.I., Nikolenko E.I., Sharygin I.S., Rezvukhina O.V., Chervyakovskaya M.V. and Korsakov A.V. (2022) Cr-pyrope xenocrysts with oxide mineral inclusions from the Chompolo lamprophyres (Aldan shield): Insights into mantle processes beneath southeastern Siberian craton. *Mineralogical Magazine*, 1–18.

Rothkirch A., Gatta G.D., Meyer M., Merkel S., Merlini M. and Liermann H.-P. (2013) Single-crystal diffraction at the Extreme Conditions beamline P02. 2: procedure for collecting and analyzing high-pressure single-crystal data. *Journal of Synchrotron Radiation*, **20**, 711–720.

Skuzovatov S., Zedgenizov D., Howell D. and Griffin W.L. (2016) Various growth environments of cloudy diamonds from the Malobotuobia kimberlite field (Siberian craton). *Lithos*, **265**, 96–107.

Sobolev N.V., Kaminsky F.V., Griffin W.L., Yefimova E.S., Win T.T., Ryan C.G. and Botkunov A.I. (1997) Mineral inclusions in diamonds from the Sputnik kimberlite pipe, Yakutia. *Lithos*, **39**, 135–157.

Stachel T., Aulbach S., Brey G.P., Harris J.W., Leost I., Tappert R. and Viljoen K.S. (2004) The trace element composition of silicate inclusions in diamonds: a review. *Lithos*, **77**, 1–19.

Varlamov D.A., Garanin V.K. and Kostrovitskiy S.I. (1996) Exotic high-titanium minerals as inclusions in garnets from lower crustal and mantle xenoliths. *Transactions of the Russian Academy of Sciences, Earth Science Section*, **345A**, 352–355.

Wang L., Essene E.J. and Zhang Y. (1999) Mineral inclusions in pyrope crystals from Garnet Ridge, Arizona, USA: implications for processes in the upper mantle. *Contributions to Mineralogy and Petrology*, **135**, 164–178.

Wang F., Fan G., Li T., Ge X., Wu Y., Wang H. and Yao J. (2021) Haitaite-(La), IMA 2019-033a. CNMNC Newsletter 60. *Mineralogical Magazine*, **85**, 454–458, https://doi.org/10.1180/mgm.2021.30

Wülser P.A., Meisser N., Brugger J., Schenk K., Ansermet S., Bonin M. and Bussy F. (2005) Cleusonite, $(Pb,Sr)(U^{4+},U^{6+})(Fe^{2+},Zn)_2(Ti,Fe^{2+},Fe^{3+})_{18}(O,OH)_{38}$, a new mineral species of the crichtonite group from the western Swiss Alps. *European Journal of Mineralogy*, **17**, 933–942.

Ziberna L., Nimis P., Zanetti A., Marzoli A. and Sobolev N.V. (2013) Metasomatic processes in the central Siberian cratonic mantle: Evidence from garnet xenocrysts from the Zagadochnaya kimberlite. *Journal of Petrology*, **54**, 2379–2409.

https://doi.org/10.1180/mgm.2023.10 Published online by Cambridge University Press